Carbon-Supported Pt and PtRu Nanoparticles as Catalysts for a Direct Methanol Fuel Cell

Zhaolin Liu,*,† Xing Yi Ling,† Xiaodi Su,† and Jim Yang Lee†,‡

Institute of Materials Research & Engineering, 3 Research Link, Singapore 117602, and Department of Chemical and Environmental Engineering, National University of Singapore, 10 Kent Ridge Crescent, Singapore 119260

Received: February 9, 2004; In Final Form: March 23, 2004

Nanosized Pt and PtRu colloids were prepared by a microwave-assisted polyol process and transferred to a toluene solution of decanthiol. Vulcan XC-72 was then added to the toluene solution to adsorb the thiolated Pt and PtRu colloids. TEM examinations showed nearly spherical particles and narrow size distributions for both supported and unsupported metals. The carbon-supported Pt and PtRu nanoparticles were activated by thermal treatment to remove the thiol stabilizing shell. All Pt and PtRu catalysts (except $Pt_{23}Ru_{77}$) showed the X-ray diffraction pattern of a face-centered cubic (fcc) crystal structure, whereas the $Pt_{23}Ru_{77}$ alloy was more typical of the hexagonal close-packed (hcp) structure. The electro-oxidation of liquid methanol on these catalysts was investigated at room temperature by cyclic voltammetry and chronoamperometry. The results showed that the alloy catalyst was catalytically more active than pure platinum. The heat-treated catalyst was also expectedly more active than the non-heat-treated ones, because of the successful removal of the organic shell, which might interfere with reactant adsorption in the methanol oxidation reaction. $Pt_{52}Ru_{48}$/C had the best electrocatalytic performance among all carbon-supported Pt and PtRu catalysts.

1. Introduction

Pt and Pt alloys are catalytically active in room temperature electro-oxidation reactions of interest to fuel cell applications. It is well-known that the catalytic activity of the metal is strongly dependent on the particle shape, size, and size distribution.[1] Conventional preparation techniques based on wet impregnation and chemical reduction of the metal precursors often do not provide adequate control of particle shape and size.[1] There is continuing effort to develop alternative synthesis methods based on microemulsions,[2] sonochemistry,[3,4] and microwave irradiation,[5−9] all of which are in principle more conducive to generating colloids and clusters on the nanoscale, and with greater uniformity.

Legratiet et al.[10] reported a significant increase in particle size when the metal content in a commercial E-TEK Pt/Vulcan catalyst is increased from 10 to 60 wt %. The metal particle size for a 10 wt % Pt catalyst was 2.0 nm but increased to 3.2 and 8.8 nm for a 30 and a 60 wt % Pt catalyst, respectively. Other studies and patents[11−14] have also underlined the difficulty of using conventional methods to preparing platinum catalysts with high metal loadings (>20 wt %) and small particle sizes (1−2 nm). In an attempt by Boennemann et al.,[15] organoaluminum-stabilized bimetallic colloids with particle size smaller than 2 nm were prepared and deposited on a commercial support at room temperature. The stabilizing surfactant shell on the metal particles had to be removed before the metal particles could be used for electrocatalysis.

In another method first used by Yu and co-workers[5] generally known as the polyol process, an ethylene glycol solution of the metal salt was refluxed at 393−443 K to generate in-situ reducing species from ethylene glycol for the reduction of the metallic species. Conductive heating is often used, but microwave dielectric loss heating may be a better synthesis option in view of its energy efficiency, speed, uniformity, and simplicity in execution.[16]

We have proposed a new method of preparing carbon-supported Pt and PtRu catalysts active in room-temperature electro-oxidation of methanol,[17] as part of our continuing work on developing low-cost processes for the preparation of homogeneous and well-defined nanoparticle catalysts for fuel cell applications. In the present work, the thiol-encapsulated Pt and PtRu colloids with different Ru contents are synthesized by a microwave-assisted polyol process and deposited on carbon and heat treated to produce carbon-supported Pt and PtRu catalysts. The crystal structure and electrochemical activities in the methanol oxidation reaction of the thiol-encapsulated Pt and PtRu colloids with different Ru contents deposited on carbon under different heat-treatment conditions will be investigated.

2. Experimental Section

Colloid Synthesis. Analytical grades of hydrogen hexachloroplatinate hydrate, ruthenium chloride, sodium hydroxide, ethylene glycol, toluene, and decanethiol were used for the synthesis. All aqueous solutions were prepared using distilled, deionized water.

A 2 mL portion of aqueous 20 mM hydrogen hexachloroplatinate hydrate solution was mixed with 25 mL of ethylene glycol to produce a yellowish solution. The solution was placed in a CEM microwave reactor with the maximum temperature set at 170 °C for 60 s. The solution changed its color from yellow to yellowish brown upon heating and was left to cool to room temperature naturally. The cooled mixture was diluted with 1−2 times its volume of distilled, deionized water. The diluted Pt colloid solution was added to 25 mL of a toluene solution of decanethiol to provide a thiol/Pt molar ratio in the

* To whom correspondence should be addressed. E-mail: zl-liu@imre.a-star.edu.sg. Fax: 65-68720785.

† Institute of Materials Research & Engineering.

‡ National University of Singapore.

10.1021/jp049422b CCC: $27.50
Published on Web 05/13/2004

range of 3−10. The biphasic mixture was vigorously stirred for a few minutes and the transfer of Pt from the ethylene glycol/water phase to toluene would occur, leaving a clear aqueous solution behind. The synthesis of the binary PtRu nanoparticles was carried out similarly, using $(1.2 - x)$ mL of 20 mM of H_2PtCl_6, x mL of 20 mM $RuCl_3$, and 25 mL of ethylene glycol in the starting mixture. x was chosen to yield initial Pt to Ru mole ratios of 0.25, 1, 2, and 4. The PtRu products were later known as $Pt_{20}Ru_{80}$, $Pt_{50}Ru_{50}$, $Pt_{67}Ru_{33}$, and $Pt_{80}Ru_{20}$, respectively, where the numerical subscripts beside Pt and Ru denote the atomic percentage of the respective alloying metal.

To determine the actual platinum and ruthenium contents in the PtRu alloys, inductively coupled plasma spectroscopy (ICP) was used to measure the unreacted metal ions remaining in the ethylene glycol−water mixtures. The PtRu alloy nanoparticles of compositions $Pt_{23}Ru_{77}$, $Pt_{52}Ru_{48}$, $Pt_{72}Ru_{28}$, and $Pt_{85}Ru_{15}$ were obtained from precursors $Pt_{20}Ru_{80}$, $Pt_{50}Ru_{50}$, $Pt_{67}Ru_{33}$, and $Pt_{80}Ru_{20}$. The ruthenium contents in the PtRu alloy nanoparticles were conspicuously lower than in the initial mixtures. This is because some Ru^{3+} ions failed to be simultaneously reduced with Pt^{4+} ions within 30 s of reaction time as the redox potential of Ru^{3+}/Ru ($E_o \sim 0.84$ V) is of much lower than that of Pt^{4+}/Pt ion ($E_o \sim 1.41$ V).[18]

Preparation of Catalysts. The stable thiol-encapsulated Pt and PtRu colloids were supported on high surface area Vulcan XC-72 carbon (as-synthesized Pt and as-synthesized PtRu colloid catalysts, 20 wt % metal content) by combining a toluene dispersion of Pt or PtRu colloid with a suspension of Vulcan carbon in toluene. The solution was vigorous stirred for 2 h. Solvent was evaporated and the solid residue was rinsed with ethanol. Finally, the powder was dried at 60 °C in a vacuum.

To remove the stabilizing shell on the nanoparticles, as-synthesized Pt and PtRu colloid catalysts were heat-treated in argon at 360 °C. The furnace was purged with argon gas for at least 15 min prior to the heat treatment. The heat-treated electrocatalysts were labeled as heated-treated Pt (x h) or PtRu (x h), where x refers to the number of hours of heat treatment (e.g., 1, 2, 5, 10 h). All prepared catalysts had a nominal metal loading of 20 wt % on the Vulcan carbon black support. The heat-treated samples are identified as heat-treated Pt and heat-treated PtRu catalysts in the following discussion.

Characterization. The Pt or PtRu colloidal formation process was monitored by UV−visible spectroscopy on a Shimadzu UV-2501 PC double beam spectrophotometer in the region 220−800 nm, using 1 cm path length quartz cuvettes. The particle morphology, size, and size distribution of the colloids and catalysts were characterized by transmission electron microscopy (TEM) using a Philips CM300 FEG system operating at 300 kV. TEM samples were prepared by placing a drop of the colloidal dispersion or a (1 h) sonicated catalyst suspension in acetone on a 3 mm Cu grid, following by drying under ambient conditions. X-ray diffraction (XRD) patterns were recorded by a Bruker GADDS diffractometer with area detector using a Cu Kα source ($\lambda = 1.540\,56$ nm) operating at 40 kV and 40 mA. XRD samples were obtained by depositing carbon-supported nanoparticles on a glass slide and drying the later in a vacuum overnight.

Electrochemical Measurement. An EG&G Model 273 potentiostat/galvanostat and a conventional three-electrode test cell were used for electrochemical measurements. The working electrode was a thin layer of Nafion-impregnated catalyst cast on a vitreous carbon disk held in a Teflon cylinder. The catalyst layer was obtained in the following way: (i) a slurry was first prepared by sonicating for 1 h a mixture of 0.5 mL of deionized water, 0.013 g of Pt/C or PtRu/C catalyst, and 0.11 g of Nafion solution (Aldrich, 5 w/o Nafion). (ii) Then 1 μL of the slurry was pipetted and spread on the carbon disk, and (iii) the electrode was then dried at 90 °C for 1 h and mounted on a stainless steel support. The surface area of the vitreous carbon disk was 0.25 cm^2. Pt gauze and a saturated calomel electrode (SCE) were used as the counter and reference electrodes, respectively. All potentials quoted in this report were referred to the SCE. All electrolyte solutions were deaerated by high-purity argon for 2 h prior to any measurement. For linear sweep voltammetry and chronoamperometry of methanol oxidation, the electrolyte solution was 2 M CH_3OH in 1 M H_2SO_4, which was prepared from high-purity sulfuric acid, high-purity grade methanol, and distilled water.

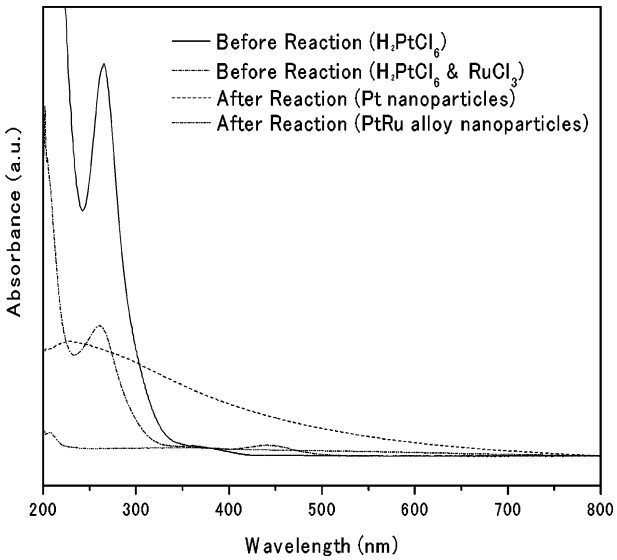

Figure 1. UV−vis absorption spectra of a solution containing H_2PtCl_6 and a mixture of H_2PtCl_6 and $RuCl_3$ before and after microwave irradiation.

3. Results and Discussion

Physicochemical Characterization of As-Synthesized Pt or PtRu Colloid and Heat-Treated Pt or PtRu Catalysts. The formation of Pt colloids via microwave dielectric heating was followed by UV−vis spectroscopy. The H_2PtCl_6 solution before microwave irradiation was pale yellow, showing a peak at 260 nm in its UV−vis spectrum (Figure 1) as a result of the ligand-to-metal charge-transfer transition in the $PtCl_6^{2-}$ ion.[19,20] The color of the solution changed to dark brown after the reaction. The peak at 260 nm was no longer visible, suggesting that all $PtCl_6^{2-}$ ions were completely reduced. The spectrum of the completely reduced solution displayed strong absorption from 700 nm and gradually increasing intensity from the visible to the ultraviolet region, confirming the formation of colloids.[21] When the Pt colloid in ethylene glycol were diluted with distilled deionized water and mixed with a toluene solution of decanethiol, transfer of Pt from the ethylene glycol/water phase to toluene took place. This was visually evident from the color change in the two phases. The color of the ethylene glycol/water solution faded gradually to colorless, whereas the color of the toluene/hexane phase darkened from colorless to yellowish brown or dark brown.

It was observed that the addition of NaOH to $RuCl_3$ (or a mixture of H_2PtCl_6 and $RuCl_3$) would cause an instant color change from dark brown to yellow-green, due to the formation of ruthenium hydroxide complexes. This was also shown

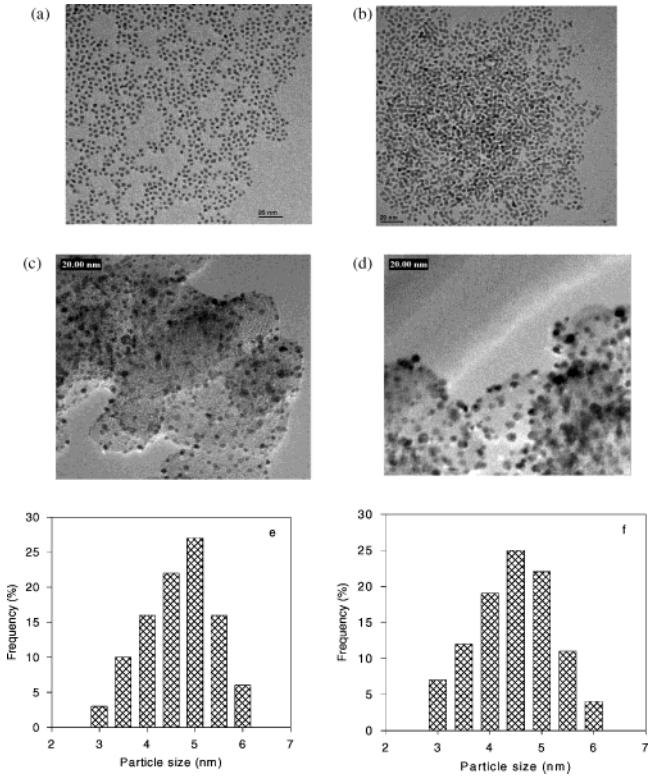

Figure 2. TEM images of the as-synthesized Pt (a) and PtRu (b) colloid catalysts and the heat-treated Pt (c) and PtRu (d) catalysts. Histograms of particle size distributions for the as-synthesized Pt (e) and PtRu (f) colloids.

spectroscopically as the evolution of a peak at ~436 nm. The observation is similar to that of Pârvulescu.[22] For PtRu alloy nanoparticle formation, characteristic absorptions by Ru^{3+} and $PtCl_6^{2-}$ ions at 436 and 260 nm disappeared and were replaced by a gradually decreasing absorption from the ultraviolet region to 700 nm, indicating the formation of PtRu nanoparticles.

Figure 2a and b are typical TEM images of the Pt and $Pt_{52}Ru_{48}$ colloids, showing remarkably uniform and highly disperse metal and alloy particles. The average diameters of 4.7 nm (for Pt) and 4.5 nm (for $Pt_{52}Ru_{48}$) were accompanied by relatively narrow particle size distributions (Figure 2e,f, range = 3−6 nm, standard deviations = 0.4 nm). Adsorption of the colloidal particles on Vulcan carbon followed by thermal treatment (in an argon gas at 360 °C for 5 h) to remove the stabilizing alkanethiol layer did not bring about significant morphological changes (Figure 2c,d). The Pt and alloy nanoparticles were in a state of high dispersion over the carbon surface, and the size of the particles was nearly unchanged.

XRD is a bulk analysis that reveals the crystal structure, lattice constants, and crystal orientation of the supported catalysts. Figure 3 shows the XRD pattern of as-synthesized Pt/C under different heat treatment conditions. The same pattern was also replicated by all heat-treated Pt/C. The strong diffraction at $2\theta < 35°$ was shown in the figure because it pertains mostly to the carbon black support. The peaks could be indexed to the [111], [200], [311], and [222] reflections of a Pt face-centered cubic (fcc) crystal structure. The lattice constant of 3.924 Å (for all Pt/C catalysts) is in good agreement with 3.923 Å for pure Pt.

The as-prepared Pt/C showed considerable crystallinity before the heat treatment. The degree of crystallization increased expectedly with the heating time, as shown by the sharper and more intense diffractions peaks. The intensity ratio of Pt[111] to C[002] diffractions, first adopted by Antolini et al.,[23] was used here for a more quantitative evaluation of the thermal enhancement effects on crystallization. From Figure 4, the ratio increased to 7.5 after 10 h of heat treatment, i.e., about a 16 times increase in crystallinity relative to the as-synthesized Pt/C.

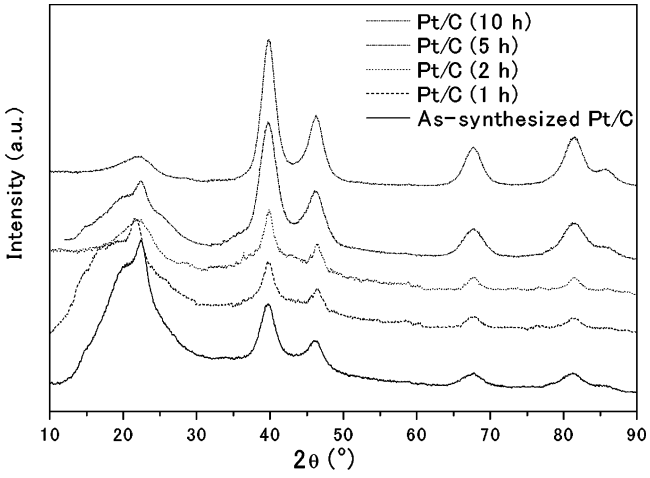

Figure 3. X-ray diffraction patterns of as-synthesized and various heat-treated Pt/C catalysts.

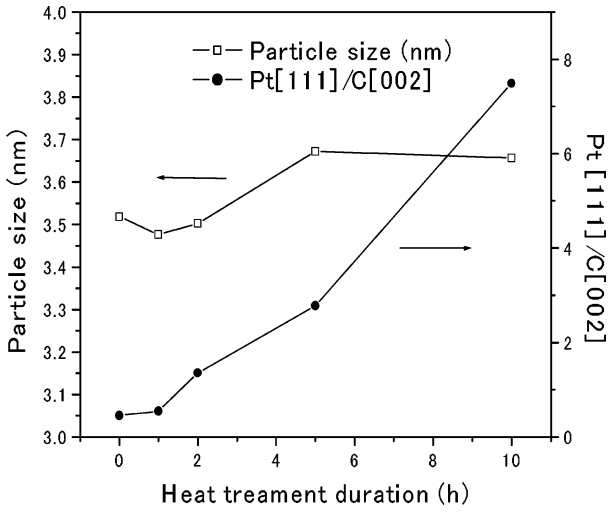

Figure 4. Particle size and crystallinity (Pt[111]/C[002]) dependence on heat-treatment duration for pure Pt catalysts.

The particle size in Figure 4 was a volume-average calculated by the Scherrer equation:

$$d\,(\text{Å}) = \frac{k\lambda}{\beta \cos\theta}$$

where k = a coefficient (0.9),

λ = the wavelength of X-ray used (1.54056 Å),

β = the full-width half-maximum of respective diffraction peak (rad),

θ = the angle at the position of peak maximum (rad).

It was found that the as-synthesized and heat-treated Pt/C had comparable particle size of 3.7 ± 0.2 nm; hence there was only a limited thermally induced particle growth in the heat treatment.

Most metal particle sizes calculated from the Scherrer equation did not agree well with the direct measurements by TEM counting 150 particles. However, the observation of nearly zero particle growth by heating in Ar was confirmed indepen-

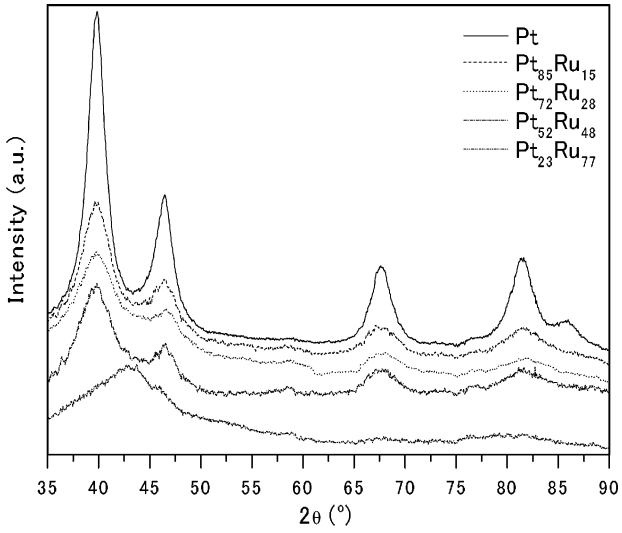

Figure 5. X-ray diffraction patterns, from top to bottom: heat-treated Pt/C, $Pt_{85}Ru_{15}$/C, $Pt_{72}Ru_{28}$/C, $Pt_{52}Ru_{48}$/C, and $Pt_{23}Ru_{77}$/C.

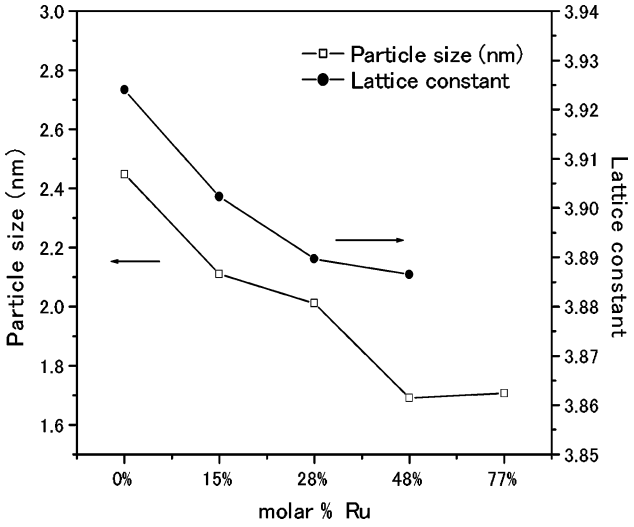

Figure 6. Dependence of particle size and lattice constant on the Ru content of heat-treated PtRu/C catalysts.

dently by TEM and XRD in more than one sample. The heat treatment produced mostly improvements in crystallinity.

XRD patterns were also collected for PtRu alloy nanoparticles supported on carbon black. Generally Ru alone would display the [100], [101], [110], [103], and [201] reflections of a hcp lattice, whereas Pt would display the characteristic fcc reflections described previously. However, from Figure 5, the diffraction pattern of heat-treated PtRu/C (except $Pt_{23}Ru_{77}$) displayed mostly the reflection characteristics of the Pt fcc structure, suggesting an alloy formation based on the substitution of the Pt lattice sites.[24] The $Pt_{23}Ru_{77}$ alloy nanoparticles were exceptional, where a hcp pattern could be clearly identified, indicating the presence of Ru-rich alloys.[25]

It was noted that with increasing proportion of Ru in the PtRu alloys, all (except $Pt_{23}Ru_{77}$) diffraction peaks were shifted synchronously to higher 2θ values. The shift is an indication of the reduction in lattice constant. According to Vegard's law, lattice constant can be used to measure the extent of alloying. In Figure 6, the lattice constant (a_o) for PtRu/C presents a decrease monotonically with the Ru content. The reduction of a_o in PtRu/C arose primarily from the substitution of platinum atoms by Ru atoms, which led to the contraction of the fcc lattice, an indication of the formation of PtRu alloys. The lattice

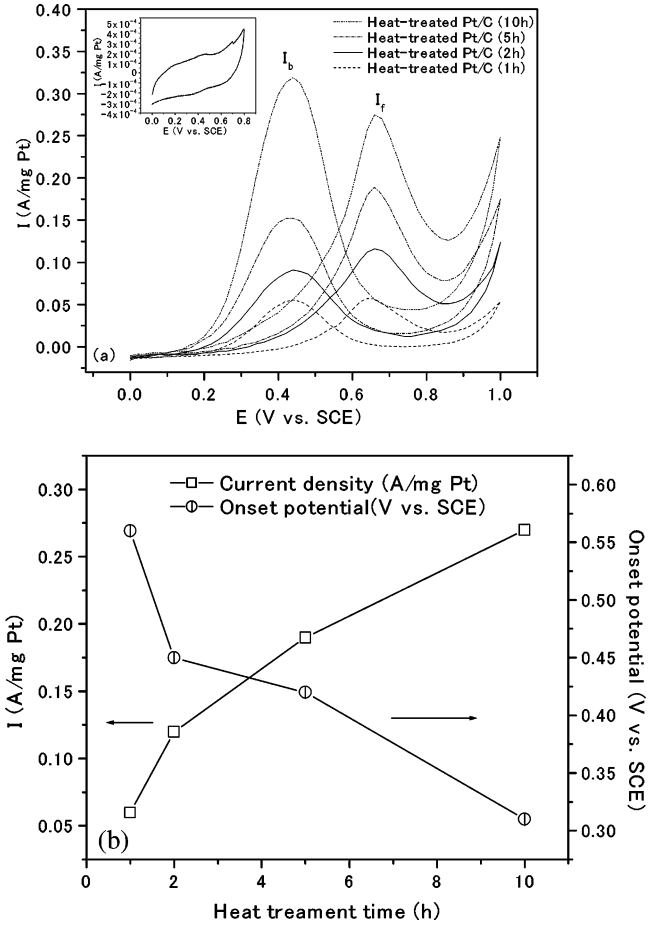

Figure 7. (a) Cyclic voltammograms of heat-treated Pt/C catalysts (1, 2, 5, 10 h) in 1 M H_2SO_4, 2 M CH_3OH electrolyte. The corresponding voltammogram of as-synthesized Pt/C is shown as an insert. (b) Plot of methanol oxidation current density as a function of heat-treatment duration.

constant contradiction also parallels the trend of decreasing particle size with increasing Ru concentration. The particle size of PtRu alloy nanoparticles falls in the order Pt > $Pt_{85}Ru_{15}$ > $Pt_{72}Ru_{28}$ > $Pt_{52}Ru_{48}$ > $Pt_{23}Ru_{77}$, which can also be explained macroscopically by the incorporation of smaller Ru atoms into the Pt nanoparticle.

Electrochemical Performances. The as-synthesized and heat-treated Pt/C catalysts (~3.7 nm) were characterized by cyclic voltammetry (0−1 V, 50 mV/s) in an electrolyte of 1 M H_2SO_4 and 2 M CH_3OH, and the resulting voltammograms are shown in Figure 7a. The as-synthesized Pt/C catalyst displayed an almost featureless voltammogram with low current density values throughout. This indicated that the Pt surface was fully covered and passivated by a shell of thiol molecules, which limited the access of the electrolyte to the catalytically active sites. Comparing the activities of the non-heat-treated catalyst (as-synthesized Pt colloid catalyst) with the corresponding heat-treated catalyst (heat-treated Pt catalyst), methanol oxidation was easier with the heat-treated sample, after the removal of the thiol stabilizing shell. Heat treatment could in principle also induce particle growth and enhance crystallization, but this was not observed experimentally because of substrate stabilization from the carbon support.

The voltammograms of methanol oxidation on all heat-treated Pt/C catalysts were very similar to that of the bulk Pt electrode. In the forward scan, methanol oxidation produced a prominent symmetric anodic peak around 0.65 V. As shown in Figure 7b, the anodic peak current density increased with the heat treatment

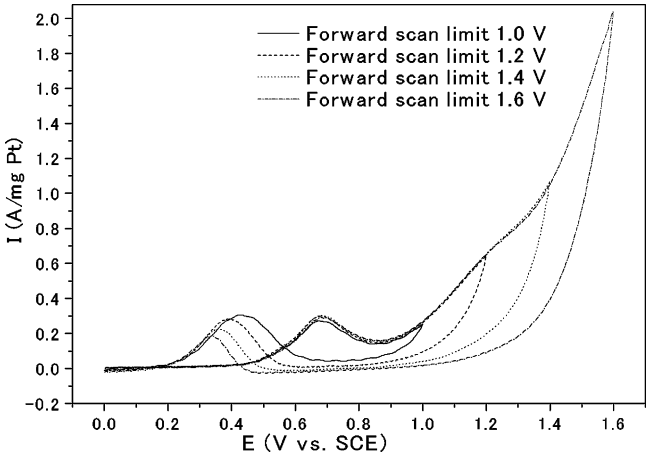

Figure 8. Cyclic voltammograms of room-temperature methanol oxidation on heat-treated Pt/C catalysts in 1 M H_2SO_4, 2 M CH_3OH at 50 mV/s for different forward potential scan limits.

time. The improved catalytic activity is obviously due to the removal of the thiol stabilizing shell by heat treatment. In the reverse scan, an anodic peak current density was detected at around 0.44 V. Goodenough et al. attributed this anodic peak in the reverse scan to the removal of the incompletely oxidized carbonaceous species formed in the forward scan.[26] These carbonaceous species are mostly in the form of linearly bonded Pt═C═O. Hence the ratio of the forward anodic peak current density (I_f) to the reverse anodic peak current density (I_b), I_f/I_b, can be used to describe the catalyst tolerance to carbonaceous species accumulation. Low I_f/I_b ratio indicates poor oxidation of methanol to carbon dioxide during the anodic scan and excessive accumulation of carbonaceous residues on the catalyst surface. High I_f/I_b ratio shows the converse case. Experimentally, the ratio was 0.87 for the heat-treated Pt/C (10 h). Such a low value indicates that a large amount of intermediate carbonaceous species was not oxidized to carbon dioxide in the forward scan. The anodic peak current density ratios for all heat-treated Pt/C catalysts were about the same when steady state was established. These experimental observations highlighted the major deficiency of pure Pt catalysts, i.e., the accumulation of intermediate carbonaceous species on the catalysts surface leading to "catalyst poisoning".

From Figure 7b, a comparison of onset potentials (the potential where $I \geq 0.025$ A/mg Pt) for methanol oxidation on all heat-treated catalysts at steady state shows that the heat-treated Pt/C (10 h) catalyst had the lowest value (0.31 V). The long heat treatment time had apparently activated the Pt the most because of a more complete removal of the protecting thiol layer.

The effect of the potential scan limit on the backward scan current is shown in Figure 8. Since the backward scan peak current decreases with increasing the anodic limit in the forward scan, it appears that the backward scan peak is primarily associated with residual carbon species on the surface rather than to the oxidation of freshly chemisorbed species. The reaction of the backward scan peak as mentioned by Goodenough et al.[26] would be written as

$$PtOH_{ad} + Pt{=}C{=}O \rightarrow CO_2 + 2Pt + H^+ + e^-$$

Hence the I_f/I_b ratio increases with the anodic limit.

The heat-treated Pt/C (1 and 10 h) catalysts were biased at 0.4 V vs SCE, and the changes in the oxidation current density with time were recorded (Figure 9). Prior to the electrochemical

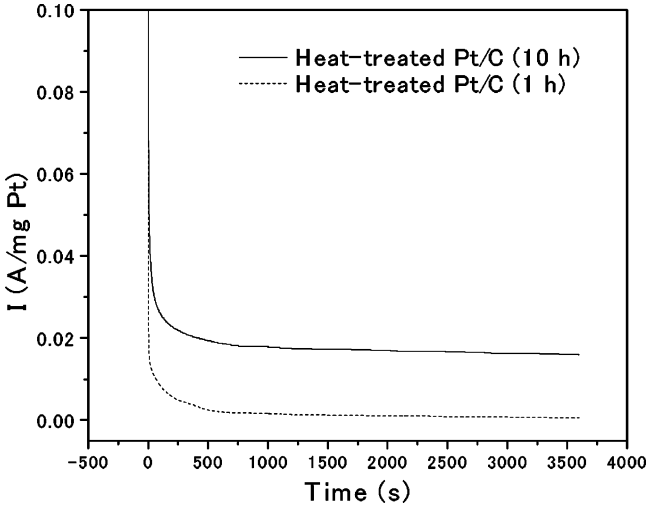

Figure 9. Comparison of the heat-treated Pt/C (1 and 10 h) catalysts for the room-temperature electro-oxidation of methanol in 1 M H_2SO_4, 2 M CH_3OH at 0.4 V (vs SCE).

endurance test, the electrolyte (1 M H_2SO_4, 2 M CH_3OH) was deaerated by Ar for at least 1 h. The working electrodes were also pretreated as follows: The potential was stepped up from the open circuit condition to 0.8 V. Two seconds later, the potential was instantaneously lowered to 0.15 V for 2 s to remove the adsorbed oxides or hydroxides[27] formed on electrode at 0.8 V. Normal recording of the current transients then proceeded with the step up to 0.4 V, which was maintained for 3600 s.

As shown in Figure 9, the current density decayed with time and reached an apparent steady state within 500 s. The heat-treated Pt/C (10 h) catalysts had higher current density values at all corresponding potentials, attesting to the advantage of a longer heat-treatment time.

Methanol oxidation on heat-treated Pt/C (10 h) and PtRu/C (10 h) catalysts with different Ru contents was compared in the following areas to indicate the catalytic performance: onset potential of methanol oxidation, anodic peak potential, ratio of the forward anodic peak current density (I_f) to the reverse anodic peak (I_b), and chronoamperometry.

Except for the $Pt_{23}Ru_{77}$/C catalyst, there was no significant feature difference between the voltammograms of carbon-supported Pt and of carbon-supported PtRu catalysts (Figure 10). Anodic peaks appeared in both the forward and reverse (cathodic) scans. The peak current density of methanol oxidation over heat-treated PtRu/C catalysts (except $Pt_{23}Ru_{77}$/C) was somewhat lower than that of heat-treated Pt/C catalyst (in the order Pt > $Pt_{52}Ru_{48}$ > $Pt_{72}Ru_{18}$ > $Pt_{85}Ru_{15}$). This is understandable, as alloying by Ru would cause a dilution of the platinum concentration on the catalyst surface. The anodic peak potential was observed to shift cathodically with the increase in the ruthenium content of the alloy (from pure Pt up to $Pt_{52}Ru_{48}$/C). $Pt_{23}Ru_{77}$/C, on the other hand, was a relatively inactive catalyst toward methanol oxidation (there was virtually no anodic peak).

As shown in Table 1, the onset potential for heat-treated Pt/C was detected at 0.31 V, whereas it was 0.15 and 0.16 V for $Pt_{85}Ru_{15}$/C and $Pt_{72}Ru_{18}$/C, respectively. When the mole percent of ruthenium was increased to 48%, i.e., heat-treated $Pt_{52}Ru_{48}$/C, the onset potential was lowered dramatically to 0.02 V. However, when the mole percent of ruthenium was further increased to 77%, the onset potential shifted positively to 0.25 V.

As stated previously, the anodic peak in the backward scan, which indicates the removal of carbonaceous species not

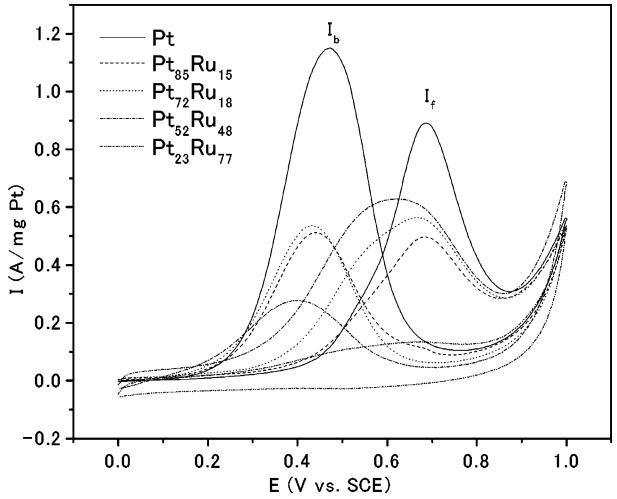

Figure 10. Cyclic voltammograms of room-temperature methanol oxidation on heat-treated Pt/C and PtRu/C catalysts in 1 M H_2SO_4, 2 M CH_3OH at 50 mV/s.

TABLE 1: Onset Potentials, Peak Potentials, and I_f/I_b Ratios of Heat-Treated Pt/C and PtRu/C

	potentials (V)		
catalyst	onset	anodic peak	I_f/I_b ratio
Pt/C	0.31	0.69	0.87
$Pt_{85}Ru_{15}$/C	0.16	0.69	0.95
Pt_{72}Ru18/C	0.15	0.66	1.06
$Pt_{52}Ru_{48}$/C	0.02	0.62	2.30
$Pt_{23}Ru_{77}$/C	0.25	na[a]	na

[a] Not applicable.

completely oxidized in the anodic scan,[26] can be used to form the ratio of anodic current density, I_f/I_b. The heat-treated Pt/C catalyst had the lowest I_f/I_b ratio (Table 1), consistent with the known low CO tolerance of Pt catalysts. The catalyst with the least carbonaceous accumulation, and hence most "tolerant" toward CO poisoning, was $Pt_{52}Ru_{48}$/C, which had the anodic current density ratio of 2.30. This can be attributed to the presence of Pt−Ru pair sites on the catalysts surface: Ru is known to adsorb oxygen-containing species (i.e., carbonaceous species) more favorably than pure Pt. However, in Ru-rich catalysts ($Pt_{23}Ru_{77}$/C), the electrochemical activity became virtually inactive mainly because ruthenium plays a role in dissociation of carbonaceous species, not in promotion of methanol oxidation reaction.

Figure 11 shows that the pattern of current decay was different for each catalyst. For heat-treated Pt/C, the current decayed continuously even after 1 h, supposedly because of catalyst poisoning by the chemisorbed carbonaceous species. The heat-treated $Pt_{52}Ru_{48}$/C (indicated as d) was able to maintain the highest current density for over 1 h among all the catalysts. The electroactivity of $Pt_{85}Ru_{15}$, $Pt_{72}Ru_{18}$ and $Pt_{23}Ru_{77}$ catalysts was worse than that of pure Pt; this would be due to ruthenium dissolution over long electrochemistry time. The comparative tests concluded that $Pt_{52}Ru_{48}$/C had the best electrocatalytic performance among all carbon-supported Pt-based catalysts prepared in this paper.

4. Conclusion

Pt and PtRu nanoparticles supported on Vulcan XC-72 carbon were prepared by a microwave-assisted polyol process. In this process Pt and PtRu colloids were first formed in an ethylene glycol solution and subsequently transferred to toluene using decanethiol as the phase-transfer agent. The metal particles prepared this way were nanosized (4.7 nm for Pt and 4.5 nm for PtRu) and had relatively narrow particle size distributions (range ∼ 3−6 nm, standard deviation ∼ 0.4 nm). XRD analysis showed that the as-synthesized Pt already had considerably crystallinity before the heat treatment, which was further refined by the heat treatment. All PtRu/C catalysts (except $Pt_{23}Ru_{77}$) displayed the characteristic diffraction peaks of the Pt fcc structure, but the 2θ values were all shifted to slightly higher values. The metal colloids were adsorbed on Vulcan CX-72 carbon and heat-treated to remove the decanethiol shell. The resulting catalysts were active in the room-temperature electro-oxidation of methanol (except $Pt_{23}Ru_{77}$/C), especially the bimetallic alloy system of $Pt_{52}Ru_{48}$. The binary catalyst was more active than the Pt-only catalyst and less receptive to methanolic residue deactivation, as expected from the bifunctional mechanism of alloy catalysts.

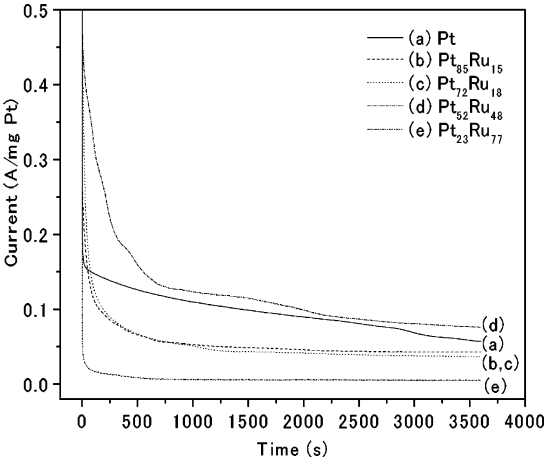

Figure 11. Comparison of the heat-treated Pt and PtRu catalysts for the electro-oxidation of methanol in 2 M CH_3OH, 1 M H_2SO_4 electrolyte at 0.4 V (vs SCE) at room temperature.

References and Notes

(1) Armadi, I. S.; Wang, Z. L.; Green, T. C.; Henglein, A.; El-Sayed, M. A. *Science* **1996**, *272*, 1924.
(2) Liu, Z. L.; Lee, J. Y.; Han, M.; Chen, W. X.; Gan, L. M. *J. Mater. Chem.* **2002**, *12*, 2453.
(3) Okitsu, K.; Yue, A.; Tanabe, S.; Matsumoto, H. *Chem. Mater.* **2000**, *12*, 3006.
(4) Fujimoto, T.; Teraushi, S.; Umehara, H.; Kojima, I.; Henderson, W. *Chem. Mater.* **2001**, *13*, 1057.
(5) Yu, W. Y.; Tu, W. X.; Liu, H. F. *Langmuir* **1999**, *15*, 6.
(6) Tu, W. X.; Liu, H. F. *Chem. Mater.* **2000**, *12*, 564.
(7) Komarneni, S.; Li, D. S.; Newalkar, B.; Katsuki, H.; Bhalla, A. S. *Langmuir* **2002**, *18*, 5959.
(8) Chen, W. X.; Lee, J. Y.; Liu, J. L. *Chem. Commun.* **2002**, 2588.
(9) Liu, Z. L.; Lee, J. Y.; Chen, W. X.; Han, M.; Gan, L. M. *Langmuir* **2004**, *20*, 181.
(10) Legratiet, B.; Remita, H.; Picq, G.; Delcourt, M. O. *J. Catal.* **1996**, *164*, 36.
(11) Gamez, A.; Richard, D.; Gallezot, P.; Gloaguen, F.; Faure, R.; Durand, R. *Electrochim. Acta* **1996**, *41*, 307.
(12) Watanabe, M.; Sakairi, K. U.S. Patent 5,728,485, 1998.
(13) Tsurumi, K.; Stonehart, P. U.S. Patent 5,480,851, 1995.
(14) Stonehart, P. U.S. Patent 5,593,934, 1997.
(15) Boennemann, H.; Binkmann, R.; Britz, P.; Endruschat, U.; Moertel, R.; Paulus, U. A.; Feldmeyer, G. J.; Schmidt, T. J.; Gasteiger, H. A.; Behm, R. J. *J. New Mater. Electrochem. Systems* **2000**, *3*, 199.
(16) Galema, S. A. *Chem. Soc. Rev.* **1997**, *26*, 233.
(17) Liu, Z. L.; Ling, X. Y.; Lee, J. Y.; Su, X. D.; Gan, L. M. *J. Mater. Chem.* **2003**, *13*, 3049.
(18) Cotton, F. A.; Wildinson, G. *Advanced Inorganic Chemistry*; John Wiley & Sons Inc.: New York, 1988.
(19) Teranishi, T.; Hosoe, M.; Tanaka, T.; Miyake, M. *J. Phys. Chem. B* **1999**, *103*, 3818.

(20) Zhao, S. Y.; Chen, S. H.; Wang, S. Y.; Li, D. G.; Ma, H. Y. *Langmuir* **2002**, *18*, 3315.
(21) Furlong, D. N.; Launikonis, A.; Sesse, W. H. F.; Sanders, L. V. *J. Chem. Soc., Faraday Trans. 1* **1984**, *80*, 571.
(22) Pârvulescu, V. I.; Coman, S.; Palade, P.; Macovei, D.; Teodorescu, C. M.; Filoti, G.; Molina, R.; Poncelet, G.; Wagner, F. E. *Appl. Surf. Sci.* **1999**, *141*, 164.
(23) Antolini, E.; Cardellini, F. *J. Alloy. Compd*. **2001**, *315*, 118.
(24) Antolini, E.; Giorgi, L.; Cardellini, F.; Passalacqua, E. *J. Solid State Electrochem.* **2001**, *5*, 131.
(25) Chu, D.; Gilman, S. *J. Electrochem. Soc.* **1996**, *143*, 1685.
(26) Manohara, R.; Goodenough, J. B. *J. Mater. Chem*. **1992**, *2*, 875.
(27) Jiang, J.; Kucernak, A. *J. Electroanal. Chem*. **2003**, *543*, 187.